Journal of Hazardous Materials 185 (2011) 29–37

Contents lists available at ScienceDirect

Journal of Hazardous Materials

journal homepage: www.elsevier.com/locate/jhazmat

Defluoridation behavior of nanostructured hydroxyapatite synthesized through an ultrasonic and microwave combined technique

Gérrard Eddy Jai Poinern[a,*], Malay K. Ghosh[c], Yan-Jing Ng[a], Touma B. Issa[b], Shashi Anand[b], Pritam Singh[b]

[a] Murdoch Applied Nanotechnology Research Group, School of Engineering and Energy, Murdoch University, South Street Perth Western Australia, WA 6150, Australia
[b] School of Chemical and Mathematical Sciences, Murdoch University, South Street Perth Western Australia, WA 6150, Australia
[c] Institute of Minerals and Materials Technology, Bhubaneswar 751013, Orissa, India

ARTICLE INFO

Article history:
Received 17 December 2009
Received in revised form 20 August 2010
Accepted 22 August 2010
Available online 7 October 2010

Keywords:
Adsorption
Defluoridation
Nanohydroxyapatite
Fluoride
Ultrasonic irradiation
Microwaves

ABSTRACT

The absorption performance of a nano-structured hydroxyapatite produced from a combined ultrasonic and microwave technique was examined for the removal of fluoride from contaminated water. The effect of physical and chemical parameters such as initial pH, contact time, initial fluoride concentration and temperature were investigated. The results indicated that the equilibrium adsorption data followed both the Langmuir and Freundlich isotherms, with a maximum monolayer adsorption capacity of 5.5 mg/g at 298 K. In addition, the kinetic studies have shown that the fluoride adsorption data followed a pseudo-second order model and that the intra-particle diffusion process played a significant role in determining the rate. The thermodynamic analysis also established that the adsorption process was endothermic and spontaneous. The initial and final fluoride loaded nano-hydroxyapatite samples were characterized using FESEM, TEM, XRD, FTIR and XPS methods. The analysis revealed that structural changes to the adsorbent had taken place.

1. Introduction

Fluoride is an essential micronutrient for human health and is usually ingested through food and drinking water. The World Health Organisation (WHO), recommends that the maximum permissible fluoride level in drinking water should not exceed 1.5 mg/L. Below this level, fluoride has a beneficial effect that results from its ability to delay dental decay [1]. Above this level, the higher concentrations of negatively charged fluoride ions are highly attracted to the positively charged calcium ions found in bones and teeth. These elevated concentrations produce serious health problems that result in skeletal fluorosis [2]. In addition, the formation of lesions in various body organs such as the endocrine glands, liver, and thyroid can also take place. The groundwater in many parts of the world exceeds the permissible fluoride level set by the WHO and as a result the de-fluoridation of contaminated water has become a critical health issue. The de-fluoridation processes currently in use can be broadly classified into either ion exchange/adsorption [3,4] or coagulation and precipitation [5]. And recently, electrodialytic membrane technologies have demonstrated their possible use for the removal fluoride from contaminated water [6].

The most extensively used de-fluoridation process used is the adsorption process. This is due to its easy operational procedure and cost-effectiveness. Many naturally occurring minerals have been tested for possible use as an adsorbent [7]. Das et al. [8] and Kamble et al. [9] have demonstrated that many naturally occurring minerals can be activated, either thermally or chemically to increase their fluoride adsorption capacity.

Hydroxyapatite (HAp) is a naturally occurring mineral found in both bone and skeletal hard tissues. It has been chemically synthesized and used for the removal of fluoride from contaminated water by several researchers [10–12]. Sundaram et al. was able to produce nano-HAp (200 nm, diameter), from a calcium hydroxide slurry by adding orthophosphoric acid and then calcining the precipitate at 400 °C. Adsorption testing was then carried out using an initial fluoride solution of 10 mg/L. The resulting adsorption capacity of the nano-HAp was found to be 1.845 mg F^-/g when the experimental testing was carried out at a pH of 3.0 [13]. Other researchers have investigated alternative forms of apatites, for example Gao et al. has examined the de-fluoridation behaviour of four different types of apatites, namely synthesized nano-HAp, bone meal, treated bone meal and rock phosphate [11]. Attempts have also been made to synthesize composite materials composed of HAp and other materials for possible use in the removal of fluoride from drinking water [14].

The manufacture of nano-HAp has been extensively investigated and several techniques, such as hydrothermal [15], sol–gel

* Corresponding author. Tel.: +61 8 9360 2892; fax: +61 8 9360 6183.
E-mail address: g.poinern@murdoch.edu.au (G.E.J. Poinern).

0304-3894/$ – see front matter © 2010 Elsevier B.V. All rights reserved.
doi:10.1016/j.jhazmat.2010.08.087

[16], emulsion and micro-emulsion [17] have been used to produce nano-HAp. However, the most attractive technique for the preparation of nano-HAp is the wet chemical method. This is because of its simplicity and economically efficient manufacturing process. Using this method allows the size and morphology of the nano-HAp particles to be controlled by simply varying the experimental conditions that regulate the particle nucleation, the aging process and the growth kinetics of the particles. Ultrasonic irradiation has also been used to synthesise several other nano-materials [18,19]. The ultrasonic technique works on the principle of generating acoustic cavitations that produce adiabatic bubbles that grow and then implosively collapse creating localized hot spots. These localised hot spots can reach temperatures of up to 5300 K and can attain pressures around 500 atmospheres, which are then followed by rapid cooling rates often exceeding 1010 K/s [20]. These extreme pressure and temperature variations promote both physical effects and chemical reactions that can directly influence the particle size and morphology of synthesised products [21,22]. Another technique that has successfully been used to synthesise materials utilises microwave heating. Meejoo et al. have discussed the use of microwave heating to dramatically reduce the reaction times and increase the product yields when compared to conventional heating methods [23]. A combined ultrasonic and microwave technique is used in this study to produce a more efficient route to manufacture nano-HAp powders. Initially, solutions containing calcium, hydroxyl and phosphate ions are irradiated by ultrasound, this results in the formation of calcium phosphate compounds. These compounds are then thermally treated using a microwave oven to produce nano-HAp.

In this study, nano-HAp was manufactured using a combined ultrasonic/microwave technique. The nano-HAP powders were characterized using X-ray diffraction (XRD), field emission scanning electron microscopy (FESEM), transmission electron microscopy (TEM), Fourier transform infrared spectroscopy (FTIR) and X-ray photoelectron spectroscopy (XPS). The adsorption capacity of the nano-HAp was investigated for the de-fluoridation of fluoride contaminated water using a batch equilibrium procedure. The various physical and chemical parameters such as pH, contact time, initial fluoride concentration and temperature were varied as part of the study to investigate their effects on the fluoride adsorption capability of the nano-HAp material. In addition, both the kinetic and thermodynamic effects of the fluoride adsorption mechanism of the nano-HAp material has been investigated and discussed.

2. Experimental

2.1. Materials

All analytical grade reagents used in this work were supplied by CHEM-SUPPLY. The chemicals used in the synthesis process were calcium nitrate tetrahydrate [$Ca(NO_3)_2{\cdot}4H_2O$], potassium dihydrogen phosphate [KH_2PO_4] and a solution of 35% ammonia. Analytical grade sodium fluoride (NaF) was used to prepare the 1000 mg/L fluoride stock solution, which was then used to prepare the diluted solution for each of the batch adsorption studies. The fluoride analysis used two standard solutions; the first was a 100 mg/L fluoride standard and the second was a Total Ionic Strength Adjustment Buffer III (TISAB III) concentrate supplied by Orion Ionplus®.

2.2. Synthesis of nano-HAp

The manufacture of nano-HAp begins initially with a 40 mL solution of 0.32 M [$Ca(NO_3)_2{\cdot}4H_2O$], then adjusting its pH to 9.0 with approximately 2.5 mL of ammonium hydroxide. The solution was then exposed to an ultrasonic irradiation source of 50 W (30 kHz) at maximum amplitude for 1 h. The ultrasonic processor (Model UP50H) was supplied by Hielscher Ultrasound Technology. Then a 60 mL solution of 0.19 M [KH_2PO_4] was added drop-wise into the initial solution while undergoing a second hour of ultrasonic irradiation.

During the synthesis process the Ca:P ratio was maintained at 1.67. After the ultrasound irradiation stage, the resultant white slurry was placed into a fused silica crucible supplied by Rojan Advanced Ceramics Pty Ltd., Western Australia. The crucible was then placed into a commercial household microwave (1100 W at 2450 MHz – LG® Australia) for heat treatment. The heat treatment continued until a white agglomerated mass was produced. This mass was then allowed to cool before being ground into a fine powder. The powder was then characterized before being used in the batch adsorption studies.

2.3. Characterization

The Brunauer–Emmett–Teller (BET) surface area measurement of the nano-HAp powders were carried out by the Australian Commonwealth Scientific and Research Organisations (CSIRO) Particle Analysis Service (PAS) in Perth, Western Australia.

The morphological features of the synthesised nano-HAp were investigated using a high resolution FESEM (Zeiss 1555 VP-FESEM) at 3 kV with a 30 μm aperture operating under a pressure of 1×10^{-10} Torr.

The powder XRD spectra of the nano-HAp powders were recorded using a Siemens D500 series diffractometer [Cu Kα = 1.5406 Å radiation source] operating at 40 kV and 30 mA. The diffraction patterns were collected at room temperature over a 2θ range from 20° to 70° with an incremental step size of 0.04°. The acquisition time was 2 s. The size of the synthesized nano-HAp powders were calculated from the respective XRD patterns using the Debye–Scherrer equation and also estimated from the FESEM micrographs.

FTIR spectral investigations were carried out using a Thermo Scientific Nicolet 6700 FTIR spectrometer. The KBr pellet technique was used and the spectra data was recorded from 4000 cm^{-1} to 400 cm^{-1} with a resolution of 4 cm^{-1}. The resulting spectra were then analysed using the OMNIC® software package.

The TEM investigation of a typical nano-HAp powder started with the powder being ground and then a small amount of the powder was dispersed in ethyl alcohol using a low powered sonic bath. Once thoroughly dispersed, the suspension was then deposited onto a carbon coated copper TEM grid and allowed to dry for 24 h. A bright field TEM study was then carried out at 80 kV using a Phillips CM-100 Electron microscope.

The Kratos Axis-Ultra spectrometer was used to obtain high resolution XPS scans using an Mg Kα X-ray source (1253.6 eV). The operating voltage was set at 12 kV with a 12 mA emission current. The pass energy of the initial survey scan was 80 eV, while the pass energy of 20 eV was used for the subsequent high resolution scans of the F 1s, O 1s, C 1s, Ca 2p and P 2p modes. The lens mode was set to 0° hybrid mode, while the magnetic lens utilities were set to 0.355 A. In addition, charge neutralization was employed to compensate for the electron deficit in the test area of the sample surface (filament current = 1.8 A, charge balance = 3.35 V and filament bias = 1 V).

2.4. pH_{pzc} determination

A set of 250 mL Schott reagent bottles were partially filled with a 100 mL solution of 0.1 M sodium nitrate ($NaNO_3$) solution. Then the pH of each solution was adjusted so that the bottle set had a pH range from 2 to 10. Once this was done a 0.1 g of synthesized

nano-HAp was added to each bottle. The bottles were then sealed, placed into a thermostatically controlled orbital shaker, with the agitation speed set to 75 rpm and operated for 24 h. After agitation, the bottles were then allowed to equilibrate for 24 h before the final pH of each sample was taken. The measured values of the final pH were then plotted against the initial pH values and from the plot the final pH value pH_{pzc} was determined from the levelling of the plotted pH curve.

2.5. Batch adsorption studies

For the equilibrium studies a 100 mL fluoride solution was taken from the standard stock solution and placed into a clean 250 mL PVC bottle. Then a 0.1 g sample of nano-HAp was added to the solution. The bottle was then sealed and the mixture was placed into a thermostatically controlled orbital shaker. The agitation speed was set to 100 rpm and run for a predetermined period. Then the effect of solution pH was studied by adjusting the pH from 3 to 9. This was done by treating the solution with 0.1 M HCl and/or 0.1 M NaOH. The temperature was normally set to 298 K, except where temperature variation studies were carried out. After 4 h, the solid was separated from the mixture using a 0.22 μm Millipore® syringe filter unit and the residual fluoride level was measured using an ion-selective electrode probe.

Isothermal studies were carried out to investigate the effect of temperature on the adsorption process. The four isotherms used were 298, 303, 313, and 318 K. A set of seven 250 mL Schott reagent bottles were partially filled with a 100 mL fluoride solution, each with a different concentration. The fluoride concentrations prepared were 1, 5, 9, 18, 22, 30, and 35 mg/L with an initial pH of 6. Then an adsorbent dose of 1.0 g/L of nano-HAp was added to each bottle. The bottles were then sealed, placed into the thermostatically controlled orbital shaker, with the agitation speed set to 75 rpm and operated for 4 h. The kinetic studies were carried out using 10 mg/L fluoride solutions at an initial pH of 6. These solutions were then placed into a thermostatically controlled orbital shaker, with the agitation speed set to 75 rpm and agitated for several different time spans (15, 30, 45, 60, 120, 180, 300 and 420 min).

2.6. Fluoride analysis

The fluoride concentration in the solution was measured using an Orion fluoride ion-selective electrode (ISE) probe which was attached to an Orion APlus™ Benchtop pH/ISE Meter-720A (Thermo-Scientific). The initial fluoride calibration curve was prepared from a set of different dilute standards prepared from a 100 mg/L standard fluoride solution from Orion. The fluoride analysis technique consisted of placing a 20 mL aliquot of a standard or sample solution into a 50 mL plastic beaker and then adding 2 mL of the TISAB III solution. The beaker with an inserted fluoride probe was then placed onto a magnetic stirrer plate where it was stirred continuously using a teflon coated magnetic bar. The solution was stirred until the meter showed a constant potential. Then, using the calibration curve, the fluoride ion concentration in the respective sample were measured after each adsorption test.

3. Results and discussions

3.1. Characterization of HAp

The FESEM images of the synthesized nano-HAp powders revealed that the particles were predominantly agglomerated and that the individual particles appeared spherical. The particles were found to be uniform and ranged in size from 40 to 50 nm in diameter. Images of the fluoride loaded nano-HAp material have shown a distinct change in the morphology of the particles. In addition to the original spherical shape, some rod shaped particles are also seen in the fluoride loaded nano-HAp materials.

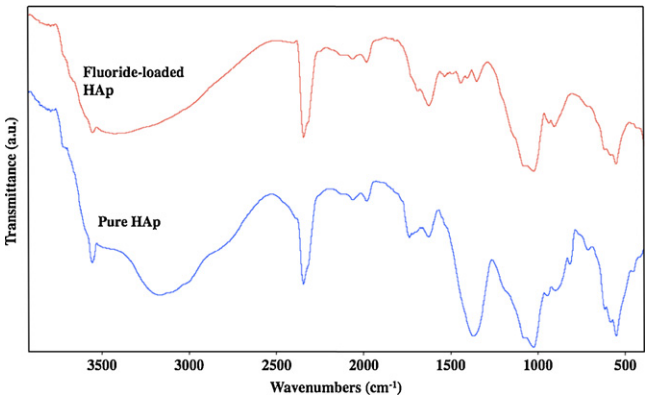

Fig. 1. FTIR spectra of n-HAp and fluoride loaded HAp.

The FTIR spectra of the synthesized nano-HAp and fluoride loaded nano-HAp powders are presented in Fig. 1. The bands around 3570 cm^{-1} and 634 cm^{-1} correspond to the characteristic stretching vibration and libration modes of the OH^- group respectively. The bands located at 1380, 825 and 725 cm^{-1} are attributed to the incorporation of CO_3^{2-} ions in the OH^- sites [24]. This is because under the highly alkaline conditions of synthesis, there are enough OH^- ions present in the aqueous system to react with the atmospheric CO_2. Typical apatite phosphate modes appear at 1090, 1040, 960, 600 and 565 cm^{-1} indicating the formation of pure apatite [22]. The phosphate bond stretching occurring at 962 cm^{-1} indicates the crystalline structure of the apatite phase formation [25]. The almost total disappearance of the CO_3^{2-} bands in the loaded sample indicates that the fluoride has been incorporated into the nano-HAp powder.

The XRD pattern of the fluoride loaded nano-HAp powders is presented in Fig. 2. It shows peaks with significant intensities at $2\theta = 25.87^\circ$ (0 0 2), 31.73° (2 1 1), 32.16° (1 1 2), 34.02° (2 0 2), 39.79° (3 1 0), 49.43° (2 1 3) and 53.09° (0 0 4). The presence of these peaks confirms the formation of HAp in the sample [22]. In addition, the presence of calcium phosphate hydrate [$Ca_3(PO_4)_2{\cdot}xH_2O$] is also indicated by the peaks at 27.09° and 29.31°. This is common in the synthesis of HAp using wet chemical methods as discussed by Poinern et al. [22]. The XRD pattern of the fluoride loaded nano-

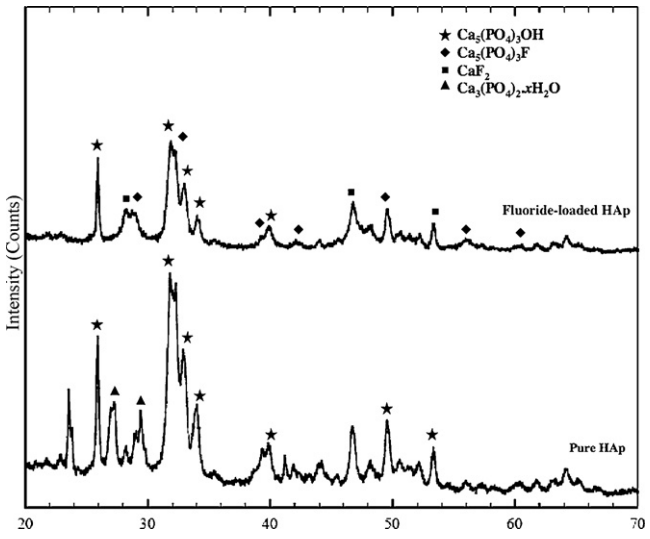

Fig. 2. XRD patterns of pure HAp (bottom) and fluoride-loaded HAp (top).

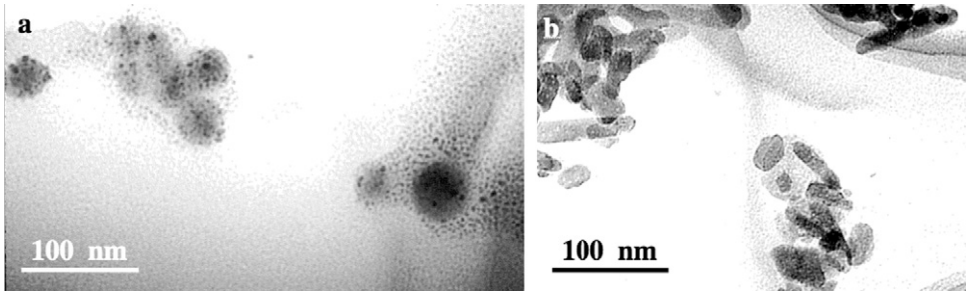

Fig. 3. TEM images of (a) pure HAp (b) fluoride loaded HAp.

HAp reveals the formation of a mixture containing HAp, fluorapatite [$Ca_5(PO_4)_3F$] and calcium fluoride (CaF_2). Contrary to the findings made by Sundaram et al. [10], this work presents the XRD patterns that indicates the formation of distinctive calcium fluoride peaks at 28.13° (1 1 1), 46.87° (2 2 0) and 55.59° (3 1 1). These peaks are in agreement with the ICDD database. The presence of fluorapatite is indicated by peaks that are similar to nano-HAp occurring at 28.92° (2 1 0), 31.85° (2 1 1), 39.97° (3 1 0), 43.81° (1 1 3), 56.02° (3 2 2) and 60.11° (4 2 0). These peaks are the result of an ion-exchange mechanism [10]. It should also be noted that the calcium phosphate hydrate peaks found in the original nano-HAp sample were not found in the fluoride loaded sample. The Debye–Scherrer equation was used to determine the average crystalline size of the nano-HAp from the XRD data. The mean size of the nano-HAp powders were calculated from the 25.87° peak [22] and found to be 43 nm, which was in agreement with the FESEM findings.

The TEM image of the synthesized nano-HAp powder and fluoride reacted nano-HAp material are presented in Fig. 3a and b. The unloaded nano-HAp presented in Fig. 3a is predominantly spherical in shape, with an average size of 40–50 nm and agrees with the morphological observations made using the FESEM. The fluoride loaded sample presented in Fig. 3b clearly indicates a change in the particle shape. In addition to the spherical shaped particles there are also some rod or plate like particles with diameters around 8–10 nm with lengths between 80 and 100 nm long. The TEM analysis clearly indicated some structural changes in the nano-HAp materials resulting from the fluoride adsorption mechanism process.

The BET surface area measurement of nano-HAp produced a value of 3.33 m^2/g. This value was lower than expected for a mesoporous hydoxyapatite. The reasons may be due to the high crystallinity of the nano-HAp powders and the extensive agglomeration of individual particles resulting from the higher irradiation power of the microwave step. The surface area of the fluoride-loaded sample was calculated to be 115.3 m^2/g. This massive increase in surface area supports the view that a major structural change has occurred during the adsorption of the fluoride ions.

The XPS wide scans for both pure nano-HAp and fluoride-nano-HAp materials are presented in Fig. 4 and were carried out to ascertain the bonding nature of the F^- adsorption process in the nano-HAp powders. The main peaks for the nominal elements are presented along with the fluoride 1s peaks that appear in the fluoride loaded nano-HAp, thus confirming the presence of the fluoride in the loaded sample. The peak energies of the peaks and possible components are presented in Table 1. The F 1s and Ca 2p peaks have been de-convoluted and presented in Fig. 5. The de-convolution of the calcium 2p peak from the fluoride loaded nano-HAp sample indicates that Ca 2p consists of two components. The first, at 346.94 eV indicates the bonding of Ca with oxygen. The second, at 347.62 eV indicates that some of the Ca has bonded with fluorine to form CaF_2. A semi-quantitative analysis has also shown that around 2% of the Ca forms CaF_2 with the F^- in the fluoride loaded nano-HAp sample. The F 1s peak at 683.67 eV indicates that about 1% of the F^- forms additional configurations with other elements, such as oxygen. It can also be seen that the 0.1 eV positive shift in the phosphorus, P 2p, peak from the original nano-HAp sample to fluoride loaded nano-HAp sample indicates the incorporation of the fluoride ions. This effect may also distort the matrix of the original nano-HAP, as well as affecting the bonding state of the P atoms. It should be noted that XPS is a surface sensitive technique, so if the CaF_2 is being bonded back to the surface of the fluoride loaded nano-HAp sample the fluoride attached inside the nano-HAp matrix will not be as prominent in the XPS spectra. The presence of CaF_2 indicates that the F^- ions to some extent do breakdown the structure of the nano-HAp during the adsorption process. This phenomenon is consistent with the XRD results presented earlier. It should also be noted that the formation of CaF_2 during fluoride adsorption by HAp has not been reported in the literature.

3.2. The effect of pH

Solution pH controls the adsorption phenomena at the water–solid interface and hence the effect of solution pH on the fluoride adsorption mechanism was studied. The study was conducted using two different initial concentration levels (10 mg/L and 50 mg/L) and by varying initial pH from 3 to 9. During the investigation the adsorbent dose (1.0 g/L), contact time (4 h) and temperature (298 K) were kept constant. The results of the study are graphically presented in Fig. 6. It can be seen that fluoride adsorption decreases as the pH increases from 3 to 5, then remains fairly constant up to 7. Beyond a pH of 7 the adsorption begins to decrease

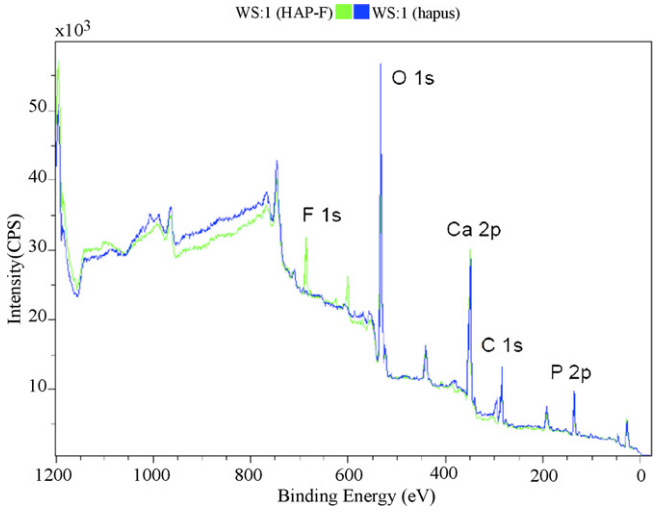

Fig. 4. Wide scan XPS spectra of pure HAp (blue) and fluoride loaded HAp (green). (For interpretation of the references to color in the figure caption, the reader is referred to the web version of the article.)

Table 1
XPS peak energies of HAp and F^- loaded HAp.

Sample	F 1s	F KLL	O 1s	Ca 2p1/2	Ca 2p3/2	C 1s	P 2p1/2	P 2p3/2
HAp			530.75M	347.0M	350.37	282.58M 285.75	132.72	133.52
HAp-F	684.65M 683.67Sh	598.09 624.0	530.85M	346.82M 347.57Sh	350.23M 351.17Sh	282.42M 285.16Sh	132.86	133.69

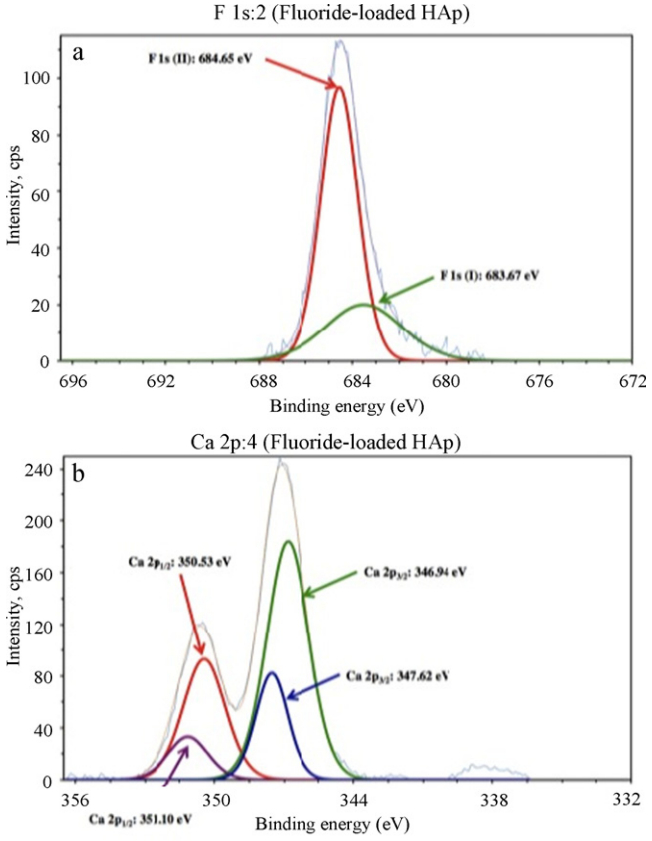

Fig. 5. XPS deconvulation of (a) Ca 2s peaks and (b) F 1s peaks.

again, especially for the lower initial concentration of 10 mg/L. The inserted graph in Fig. 6 presents the plot of the equilibrium pH (pH_{eq}) of the solution after adsorption against the initial pH (pH_i). In a recent study by Jiménez-Reyes and Solache-Rios [26], the rapid dissolution of HAp material at low values of pH was reported. For example, when the pH was 2.8 there was a rapid dissolution of HAp. It was found that when the pH was less than 4 (pH < 4), HAp formed the soluble species Ca^{2+} and $CaH_2PO_4^+$. In contrast, when the pH was greater than 4 (pH > 4) only the insoluble species $CaHPO_4{\cdot}2H_2O$ and $Ca_5(PO_4)_3OH$ were present. In our study, the pH_{in} was set at 3.0. This resulted in an equilibrium pH_{eq} of 4 and above (Fig. 6, insert) and as a result, no HAp dissolution was observed.

In the present study, pH_{pzc} was found to be 7.2 while the literature has reported values in the range from 4.35 to 7.6 [27]. Below pH_{pzc} the HAp surface is protonated and acquires a positive charge. When the pH is lower than 3.0, the higher fluoride adsorption is presumably due to the electrostatic attraction of the positively charged surface with negatively charged fluoride ions. The decrease in adsorption between pH values of 3.0 and 5.0 is due to the decrease in the positive surface charge density. Beyond pH 7.2, the surface is deprotonated and acquires a negative charge, which repels the negatively charged fluoride ions and consequently adsorption decreases. In further studies, pH_{in} 6.0 (corresponding pH_{eq} 6.6) was chosen as the optimized pH because of its close value to natural water or drinking water.

3.3. The effect of contact time

The fluoride adsorption of HAp as a function of contact time is presented in Fig. 7. During the kinetic studies the contact time was varied from 15 min to 7 h, with an initial fluoride concentration of 10 mg/L, a temperature of 298 K, an absorbent dose of 1 g/L and an equilibrium solution pH of 6.6. It is evident from inspecting Fig. 7, that the adsorption process has two distinct phases: an initial fast phase, which lasted for about 60 min followed by a much slower adsorption phase. The equilibrium time was established after approximately 3 h. Hence, all subsequent experiments were carried out over a 4 h period.

3.4. Adsorption kinetics

The solute adsorption rate determines the residence time required for completing the adsorption reaction. Therefore the kinetic analysis is essential for any absorption study. The adsorption

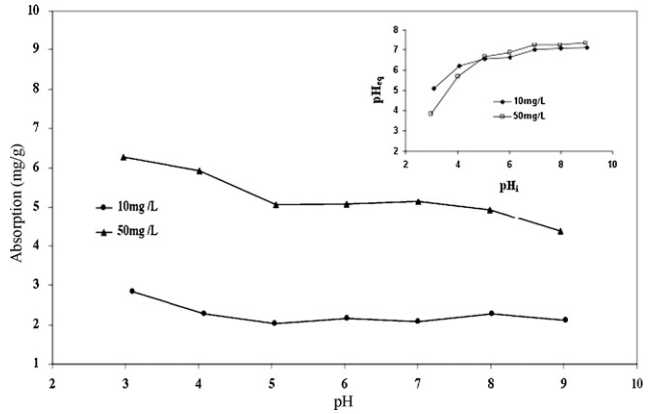

Fig. 6. Effect of pH on fluoride adsorption [conditions: 298 K, HAp dose 1.0 g/L, contact time 4 h].

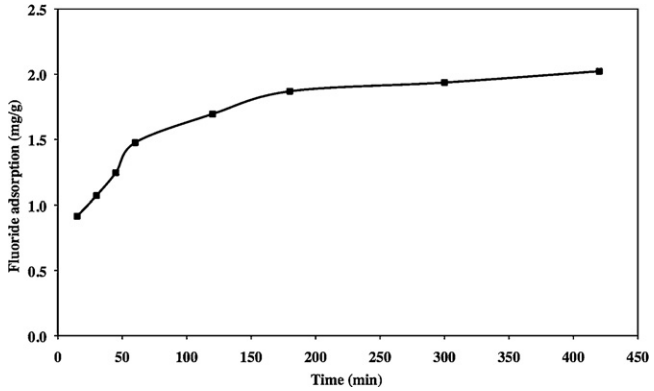

Fig. 7. Effect of contact time on fluoride adsorption by nano-HAp [conditions: equilibrium pH 6.6, 298 K, [F^-] 10 mg/L, HAp dose 1.0 g/L].

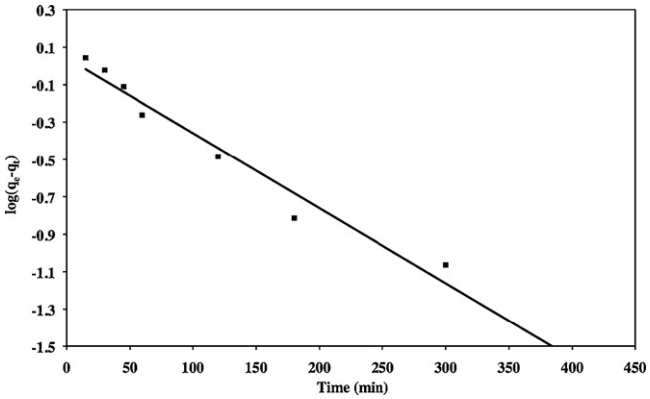

Fig. 8. Pseudo-second order plot for fluoride adsorption on nano-HAp [conditions: equilibrium pH 6.6, 298 K, [F⁻] 10 mg/L, HAp dose 1.0 g/L].

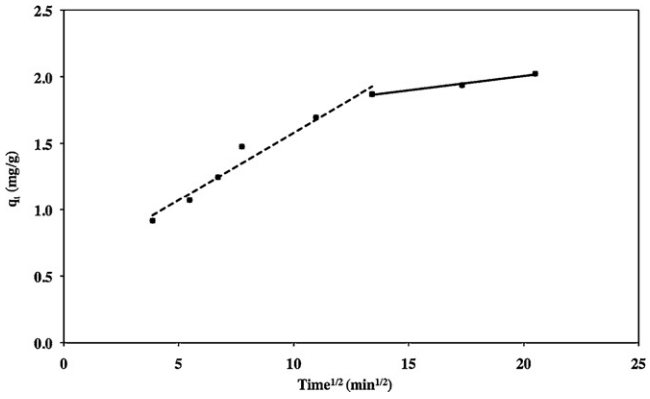

Fig. 9. Intra-particle diffusion plot of fluoride on nano-HAp.

data was analysed using three kinetic models: pseudo first order, pseudo second order and the intra-particle diffusion model.

The Lagergren pseudo-first order rate law [28] can be expressed as

$$\log(q_e - q_t) = \log q_e - \frac{k_1}{2.303}t \quad (1)$$

where q_e (mg/g) is the adsorption at equilibrium, q_t (mg/g) is the adsorption at time t and k_1(/min) is the pseudo-first order adsorption rate constant.

The pseudo-second-order rate law [29] for analysis of sorption kinetics can be expressed as

$$\frac{t}{q_t} = \frac{1}{k_2 q_e^2} + \frac{1}{q_e}t \quad (2)$$

where k_2 (g/min mg) is the pseudo-second-order rate constant for adsorption. Fig. 8 presents a graph of the kinetic data that was plotted using Eq. (2). Inspection of the graph reveals that the plot is linear.

The rate constants and other parameters obtained from plotting both kinetic models are presented in Table 2. Both models adequately fit the data obtained. However, the second order model provides a better fit as well as a higher correlation coefficient (R^2). Also, the calculated equilibrium capacity calculated from the second order model is in close agreement with the experimentally determined value.

The adsorption mechanism is a multi-step process. The first step involves the diffusion of the sorbate from the aqueous phase to the adsorbent surface. In the next step diffusion takes place in the internal pores and voids within the matrix of the absorbent. The diffusion process in this case is slow and occurs at a lower rate. Weber and Morris [30] have described an intra-particle diffusion model which is represented by the following equation:

$$q_t = k_p t^{1/2} + C \quad (3)$$

where k_p is the intra-particle diffusion rate constant (mg/g min$^{1/2}$ g) and C is the intercept which provides an idea of the boundary layer thickness.

According to this model, if intra-particle diffusion is involved in the adsorption process then the resulting plot of q_t versus $t^{1/2}$ should be linear and if the line passes through the origin then intra-particle diffusion is the sole rate-controlling step. However, if the data exhibits multi-linear plots then two or more steps may influence the adsorption process. Generally the first line, which is steeper, is credited to the external diffusion of adsorbate through the boundary layer to the surface of adsorbent (instantaneous adsorption stage). The second line, which has a smaller gradient describes the gradual adsorption stage. In this stage the intra-particle diffusion process is the dominant effect. The third linear portion of the graph is the final equilibrium stage, where the diffusion process begins to slow down due to low solute concentration.

Fig. 9 presents the adsorption data plotted using the intra-particle diffusion model discussed above. The first step is the external surface adsorption state which is attained rapidly (this line is not shown for clarity). The second step (dotted line) is credited to the intra-particle diffusion process which plays an important role in the first 3 h. The diffusion model parameters such as rate constant, intercept and correlation coefficient are presented in Table 2.

3.5. Adsorption isotherms

The adsorption isotherms describe the distribution of the adsorbate between the solution and the adsorbent when the adsorption process reaches an equilibrium state. In order to investigate the nature of the fluoride adsorption isotherm, the initial fluoride concentration was varied from 1 mg/L to 35 mg/L under fixed experimental parameters. These parameters included an equilibrium pH of 6.6, constant temperature of 298 K, 1 g/L absorbent dose and a contact time of 4 h. Fig. 10 presents the relationship between the equilibrium fluoride concentration and the de-fluoridation capacity of the nano-HAp particles. It can be seen that the adsorption capacity increases from 0.5 mg/g to 4.3 mg/g while the equilibrium fluoride concentration increases from 0.75 mg/L to 30.6 mg/L. The increase in adsorption capacity results from the increasing equilibrium fluoride concentration in the solution, which in turn produces larger numbers of fluoride ions available at the surface interface. The presence of large numbers of fluoride ions at the interface greatly enhances the adsorption process.

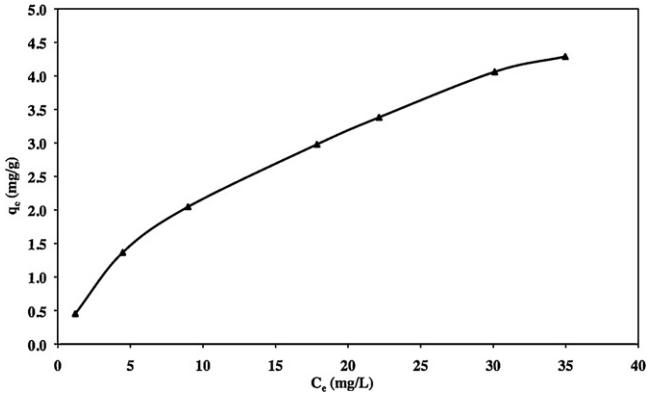

Fig. 10. Adsorption isotherm of fluoride on nano-HAp [conditions: equilibrium pH 6.6, 298 K, contact time 4 h, HAp dose 1.0 g/L].

Table 2
Rate constants and correlation coefficients of studied kinetic models.

$q_{e,exp}$ (mg/g)	Pseudo-first order			Pseudo-second order			Intra-particle diffusion		
	$q_{e,calc}$ (mg/g)	k_1 (/min)	R^2	$q_{e,calc}$ (mg/g)	k_2 (g/min mg)	R^2	k_P (mg/g min$^{1/2}$)	C (mg/g)	R^2
2.02	1.10	0.0092	0.961	2.14	0.017	0.999	0.101	0.56	0.965

There are several applicable isotherm models, but the most widely used are the Langmuir and the Freundlich models. The Freundlich model is purely an empirical one, unlike the Langmuir model which assumes the maximum adsorption occurs when the surface has been covered by a monolayer of adsorbate. The Langmuir isotherm model is expressed mathematically by the linear equation below:

$$\frac{C_e}{q_e} = \frac{1}{Q_m b} + \frac{C_e}{Q_m} \quad (4)$$

where Q_m (mg/g) is the monolayer adsorption capacity, b (L/g) is Langmuir constant which is related to the free energy of adsorption, C_e (mg/L) and q_e (mg/g) are the equilibrium concentration of adsorbate in solution and on the surface of adsorbent respectively. The Freundlich isotherm model equation in the linear form is presented below:

$$\log q_e = \log k_F + \frac{1}{n} \log C_e \quad (5)$$

where k_F [(mg/g)(mg/L)$^{-1/n}$] and n (dimensionless) are Freundlich isotherm constants related to the extent of the adsorption and to the adsorption intensity respectively.

The Langmuir isotherm equation (Eq. (4)) was applied to the adsorption data to quantify the adsorption capacity of the nano-HAp powders. The Langmuir plot of the data displayed a good linear fit and the derived parameters of slope and intercept, are presented in Table 3. In addition, the adsorption data was also plotted using the Freundlich model under the same experimental conditions. The data fitted well to the model and the equilibrium parameter values are presented in Table 3. The value of n is in the range of 1–10 and this indicates that the fluoride adsorption process is favourable on the nano-HAp powder.

Similarly other investigators have also reported correlation coefficients that are both high and close in value for the two models [7,8,11,31]. However, based on the coefficient of correlation (R^2) values in the present study, the Freundlich isotherm provided the best fit to the experimental data.

In order to assess the de-fluoridation efficiency of the synthesised nano-HAp powders in the present investigation, a comparative evaluation was made between the nano-HAp and several other materials reported in the literature, see Table 4. It can be seen from this table that the nano-HAP powder used in this study possesses a higher fluoride adsorption capacity than other similar nano-HAp's powders and many other adsorbents reported in the literature.

3.6. The effect of temperature

Isothermal studies were carried out to investigate the effect of temperature on the fluoride adsorption process. The four isotherms used were 298, 303, 313, and 318 K. Three different initial fluoride concentration levels (5, 10 and 20 mg/L) where used for each isotherm while the contact time (4 h) and adsorbent dose (1 g/L) were kept constant. During the experimental investigation it became apparent that adsorption increased with increasing temperature. This observation indicated that the fluoride adsorption by the nano-HAp was endothermic in nature. This observation is similar to those reported in the literature [11,12].

In order to test the feasibility and spontaneity of the adsorption process, the thermodynamic parameters of free energy change (ΔG°), enthalpy change (ΔH°) and entropy change (ΔS°) were calculated using the following relationships:

$$\Delta G^\circ = -RT \ln K \quad (6)$$

$$\Delta G^\circ = \Delta H^\circ - T\Delta S^\circ \quad (7)$$

Eq. (7) can be rearranged as,

$$\ln K = \frac{\Delta S^\circ}{R} - \frac{\Delta H^\circ}{RT} \quad (8)$$

where R is the universal gas constant (8.314 J/mol/K), T is the temperature in Kelvin and K is the thermodynamic equilibrium constant in units of L/g and is generally expressed as:

$$K = \frac{q_e}{C_e} \quad (9)$$

Since both ΔG° and the term RT have the unit of J/mol, the equilibrium constant K in (Eq. (9)) should be dimensionless. In order to make K dimensionless we have adopted the method suggested by Milonjic [32]. Thus the equilibrium constant K in (Eq. (9)) is replaced with the new dimensionless equilibrium constant K_0 which is expressed by;

$$K_0 = \frac{\rho q_e}{C_e} \quad (10)$$

where ρ is the density of water (~1000 g/L) and assumed to be constant over the temperature range studied and containing a low adsorbent dose.

The calculated K_0 values for the three different initial fluoride concentrations were plotted using the Van't Hoff equation (Eq. (8)) and graphically presented in Fig. 11. The estimated values of ΔH° (from the slope) and ΔS° (from the intercept) and the calculated value of ΔG° are presented in Table 5. It can be seen from this table that all the ΔG° values are negative for the set of four temperatures studies. This indicates that the fluoride adsorption is spontaneous

Table 3
Langmuir and Freundlich isotherm data.

Langmuir isotherm		Freundlich isotherm	
Q_m (mg/g)	5.53	k_F (mg/g)(mg/L)$^{-1/n}$	0.61
B (L/mg)	0.10	n	1.69
R^2	0.978	R^2	0.988

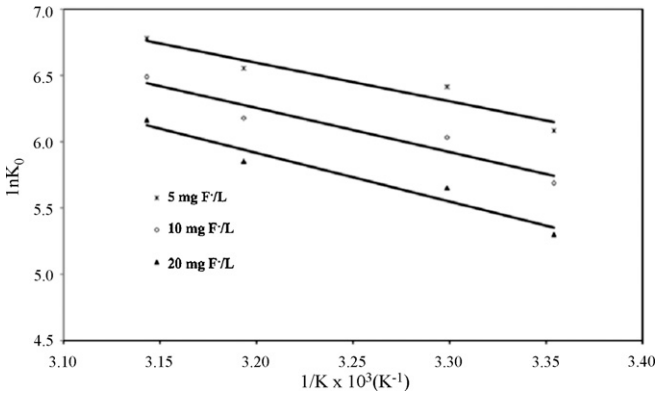

Fig. 11. Van't Hoff plot for fluoride adsorption on nano-HAp.

Table 4
Monolayer adsorption capacities of some adsorbents reported in literature.

Adsorbent	Adsorption capacity (mg/g)	Experimental conditions		Ref.
		pH (initial)	F^- concentration range (mg/L)	
n-HAp	5.5	6.0	1–35	This work
n-HAp	4.57	5.0	3–80	[11]
Bone meal	4.99			
Treated bone meal	6.85			
n-HAp	3.11	(probably) 3.0	–	[10]
Anionic clays	3.6[a]	6.5	5–60[a]	[35]
La-modified bentonite	4.24	7	0–25	[9]
Activated alumina	2.41	7	2.5–14	[36]
Precipitated waste mud	27.2	5.0	5.4–914	[31]
Acid treated waste mud	2.8			
Original waste mud	4.2			
Activated Ti-rich bauxite	3.97–4.13	6.0	5–40	[8]
Quick lime	16.67	6.6	10–100	[37]
Chromite overburden	15.17	5.0	10–50	[7]
Low iron Ni-laterite	12.3			
High iron Ni-laterite	15.17			

[a] Data converted from molar units for easy comparison.

Table 5
Thermodynamic parameters for defluoridation by nano-HAp.

Fluoride concentration (mg/L)	ΔH° (kJ/mol)	ΔS° (J/mol K)	ΔG° (kJ/mol)			
			298 K	303 K	313 K	318 K
5	24.2	132.3	−63.6	−64.3	−65.6	−66.3
10	27.6	140.3	−69.4	−70.1	−71.5	−72.2
20	30.5	146.7	−74.2	−74.9	−76.4	−77.1

in nature and the adsorption process improves with increasing temperatures.

It is known that the absolute magnitude of the free energy change for physical adsorption is less than that for chemisorption. In their studies, Jaycock and Parfitt have discussed that in the case of physical adsorption ΔG° ranges from −20 to 0 kJ/mol and in the case of chemical adsorption it ranges from −80 to −400 kJ/mol [33]. In the present study, the thermodynamic values obtained are outside the range of physical adsorption, but are closer to those of chemical adsorption. Hence in this case, this physical adsorption process has been enhanced by a chemical effect in a similar manner to that described by Yu et al. [34]. The positive value of ΔH indicates the endothermic nature of the adsorption process and the high positive value of ΔS° indicates the affinity of nano-HAp for the fluoride ions. This study suggests that there are some structural changes and points to the irreversible nature of the fluoride adsorption process with the nano-HAp material. In addition, the positive value of the enthalpy and the large positive entropy value, suggests that the entropy is responsible for making the reaction spontaneous ($-\Delta G^\circ$) and its contribution is much larger than the enthalpy change.

4. Conclusion

The results obtained in this work have demonstrated that using a combined ultrasonic and microwave irradiation technique during the wet chemical synthesis of hydroxyapatite, it is possible to produce ultrafine and highly crystalline particles of uniform size. The nano-HAp particles produced in this work were found to be very effective in the removal of fluoride ions from test solutions. The monolayer adsorption capacity was also found to be higher than other synthetic nano-HAp materials reported in the literature. The solution equilibrium pH of 6.6 after de-fluoridation is within the normal pH range for potable water. This is advantageous because there is no further need to adjust the pH for possible human consumption. The Freundlich model successfully described the adsorption data and the kinetic data fitted well to a pseudo-second order kinetic model. Thermo-chemical analysis indicates that the adsorption process is spontaneous, endothermic and that the synthesised nano-HAp possesses a high affinity towards fluoride ions.

Acknowledgements

The financial support of this work was carried out through the Australia-India Strategic Research Fund, ST01-0005. One of the authors (MKG) is grateful to Murdoch University for providing a Visiting Research Fellowship to carry out this work. The authors also wish to thank Mr. Dale Parsonage for his assistance in some parts of this project. Ms. Yan Jin acknowledges the support of the West Australian Nanochemistry Research Institute, WANRI for a research assistantship for this project. Dr. Derek Fawcett from WANRI, is thanked for his valuable contributions to this manuscript.

References

[1] A. Komárek, E. Lesaffre, T. Härkänen, D. Declerck, J.I. Virtanen, A Bayesian analysis of multivariate doubly-interval-censored dental data, Biostatistics 6 (2005) 145–155.
[2] J. Fawell, K. Bailey, J. Chilton, E. Dahi, L. Fewtrell, Y. Magara, Fluoride in Drinking-Water, 1st ed., World Health Organization (WHO), Cornwall, UK, 2006.
[3] A.M. Raichur, M.J. Basu, Adsorption of fluoride onto mixed rare earth oxides, Sep. Purif. Technol. 24 (2001) 121–127.
[4] G. Singh, B. Kumar, P.K. Sen, J. Majumdar, Removal of fluoride from spent pot liner leachate using ion exchange, Water Environ. Res. 71 (1999) 36–42.
[5] S. Saha, Treatment of aqueous effluent for fluoride removal, Water Res. 27 (1993) 1347–1350.
[6] Z. Amer, B. Bariou, N. Mameri, M. Taky, S. Nicolas, A. Elmidaoui, Fluoride removal from brackish water by electrodialysis, Desalination 133 (2001) 215–223.
[7] M.G. Sujana, H.K. Pradhan, S. Anand, Studies on sorption of some geomaterials for fluoride removal from aqueous solutions, J. Hazard. Mater. 161 (2009) 120–125.
[8] N. Das, P. Pattanaik, R. Das, Defluoridation of drinking water using activated titanium rich bauxite, J. Colloid Interface Sci. 292 (2005) 1–10.
[9] S.P. Kamble, P. Dixit, S.S. Rayalu, N.K. Labhsetwar, Defluoridation of drinking water using chemically modified bentonite clay, Desalination 249 (2009) 687–693.

[10] C.S. Sundaram, N. Viswanathan, S. Meenakshi, Defluoridation chemistry of synthetic hydroxyapatite at nano scale: equilibrium and kinetic studies, J. Hazard. Mater. 155 (2008) 206–215.
[11] S. Gao, J. Cui, Z. Wei, Study on the fluoride adsorption of various apatite materials in aqueous solution, J. Fluorine Chem. 130 (2009) 1035–1041.
[12] S. Gao, R. Sun, Z. Wei, H. Zhao, H. Li, F. Hu, Size-dependent defluoridation properties of synthetic hydroxyapatite, J. Fluorine Chem. 130 (2009) 550–556.
[13] C.S. Sundaram, N. Viswanathan, S. Meenakshi, Uptake of fluoride by nano-hydroxyapatie/chitosan, a bioinorganic composite, Bioresour. Technol. 99 (2008) 8226–8230.
[14] C.S. Sundaram, N. Viswanathan, S. Meenakshi, Fluoride sorption by nano-hydroxyapatie/chitin composite, J. Hazard. Mater. 172 (2009) 147–151.
[15] A.A. Chaudhry, S. Haque, S. Kellici, P. Boldrin, I. Rehman, F.A. Khalid, J.A. Darr, Instant nano-hydroxyapatite: a continuous and rapid hydrothermal synthesis, Chem. Commun. (2006) 2286–2288.
[16] T.A. Kuriakose, S.N. Kalkura, M. Palanichamy, D. Arivuoli, K. Dierks, G. Bocelli, C. Betzel, Synthesis of stoichiometric nano crystalline hydroxyapatite by ethanol-based sol–gel technique at low temperature, J. Cryst. Growth 263 (2004) 517–523.
[17] M.J. Phillips, J.A. Darr, Z.B. Luklinska, I. Rehman, Synthesis and characterization of nano-biomaterials with potential osteological applications, J. Mater. Sci.: Mater. Med. 14 (2003) 875–882.
[18] S. Majumdar, S. Chakraborty, P.S. Devi, A. Sen, Room temperature synthesis of nanocrystalline SnO through sonochemical route, Mater. Lett. 62 (2008) 1249–1251.
[19] B. Tanga, L. Yuana, T. Shib, L. Yua, Y. Zhu, Preparation of nano-sized magnetic particles from spent pickling liquors by ultrasonic-assisted chemical co-precipitation, J. Hazard. Mater. 163 (2009) 1173–1178.
[20] K.S. Suslick, Sonochemistry, Science 247 (4949) (1990) 1439–1445.
[21] L.-Y. Cao, C. Zhang, J.F. Huang, Influence of temperature, [Ca^{2+}], Ca/P ratio and ultrasonic power on the crystallinity and morphology of hydroxyapatite nanoparticles prepared with a novel ultrasonic precipitation method, Mater. Lett. 59 (2005) 1902–1906.
[22] G.E.J. Poinern, R.K. Brundavanam, N. Mondinos, Z. Jiang, Synthesis and characterisation of nanohydroxyapatite using an ultrasound assisted method, Ultrason. Sonochem. 16 (2009) 469–474.
[23] S. Meejoo, W. Maneeprakom, P. Winotai, Phase and thermal stability of nanocrystalline hydroxyapatite prepared via microwave heating, Thermochim. Acta 447 (2006) 115–120.
[24] Z.H. Cheng, A. Yasukawa, K. Kandori, T. Ishikawa, FTIR Study on incorporation of CO_2 into calcium hydroxyapatite, J. Chem. Soc. Faraday Trans. 94 (1998) 1501–1505.
[25] M.C. Chang, Fluoride incorporation in hydroxyapatite/gelatin nanocomposite, J. Mater. Sci. Mater. Med. 19 (2008) 2837–2843.
[26] M. Jiménez-Reyes, M. Solache-Rios, Sorption behavior of fluoride ions from aqueous solutions by hydroxyapatite, J. Hazard. Mater. 180 (2010) 297–302.
[27] L.C. Bell, A.M. Posner, J.P. Quirk, The point of zero charge of hydroxyapatite and fluorapatite in aqueous solutions, J. Colloid Interface Sci. 42 (1973) 250–261.
[28] S. Lagergren, Zur theorie der sogenannten adsorption gelöster stoffe, Kungliga Svenska Vetenskapsakademiens, Handlingar 24 (1898) 1–39.
[29] G. McKay, Y.S. Ho, Pseudo-second order model for sorption processes, Process Biochem. 34 (1999) 451–465.
[30] W.J. Weber, J.C. Morris, Kinetics of adsorption on carbon from solution, J. Sanit. Eng. Div. Am. Soc. Civ. Eng. 89 (1963) 31–60.
[31] B. Kemer, D. Ozdes, A. Gundogdu, V.N. Bulut, C. Duran, M. Soylak, Removal of fluoride ions from aqueous solution by waste mud, J. Hazard. Mater. 168 (2009) 888–894.
[32] S.K. Milonjic, A consideration of the correct calculation of thermodynamic parameters of adsorption, J. Serb. Chem. Soc. 72 (2007) 1363–1367.
[33] M.J. Jaycock, G.D. Parfitt, Chemistry of Interfaces, Ellis Horwood, Onichester, 1981.
[34] Y. Yu, Y. Zhuang, Z. Wang, Adsorption of water-soluble dye onto functionalized resin, J. Colloid Interface Sci. 242 (2001) 288–293.
[35] S. Mandal, S. Mayadevi, Defluoridation of water using as-synthesized Zn/Al/Cl anionic clay adsorbent: equilibrium and regeneration studies, J. Hazard. Mater. 167 (2009) 873–878.
[36] S. Ghorai, K.K. Pant, Equilibrium, kinetics and breakthrough studies for adsorption of fluoride on activated alumina, Sep. Purif. Technol. 42 (2005) 265–271.
[37] M. Islam, R.K. Patel, Evaluation of removal efficiency of fluoride from aqueous solution using quick lime, J. Hazard. Mater. 143 (2007) 303–310.